DISCRETE AND CONTINUOUS
DYNAMICAL SYSTEMS–SERIES B
Volume **6**, Number **6**, November **2006**

Website: http://AIMsciences.org

pp. **1357–1380**

AMPLITUDE EQUATIONS CLOSE TO A TRIPLE-(+1) BIFURCATION POINT OF $\mathbb{D}_4$-SYMMETRIC PERIODIC ORBITS IN $\mathbb{O}(2)$-EQUIVARIANT SYSTEMS

Juan Sánchez and Marta Net

Departament de Física Aplicada, Universitat Politècnica de Catalunya
Jordi Girona Salgado s/n. Campus Nord. Mòdul B4
08034 Barcelona, Spain

José M. Vega

E.T.S.I. Aeronáuticos, Universidad Politécnica de Madrid
Pl. Cardenal Cisneros 3
28040 Madrid, Spain

(Communicated by Shouhong Wang)

Abstract. A two-dimensional thermal convection problem in a circular annulus subject to a constant inward radial gravity and heated from the inside is considered. A branch of spatio-temporal symmetric periodic orbits that are known only numerically shows a multi-critical codimension-two point with a triple +1-Floquet multiplier. The weakly nonlinear analysis of the dynamics near such point is performed by deriving a system of amplitude equations using a perturbation technique, which is an extension of the Lindstedt-Poincaré method, and solvability conditions. The results obtained using the amplitude equation are compared with those from the original system of partial differential equations showing a very good agreement.

1. **Introduction.** The free thermal convection of a Boussinesq fluid in a circular annulus, subject to a constant inward radial gravity and heated from the inside is considered. This problem provides the simplest two-dimensional model for natural convection in the equatorial plane of atmospheres and planetary interiors (see [9], and the introduction of [12]). Since the problem is independent of the axial coordinate z, only roll-like structures, which are exact solutions for a cylindrical annulus subject to stress-free and perfectly conducting top and bottom boundaries [1], and perturbations keeping the two-dimensionality are studied.

Beyond the physical relevance of the problem, the z-independent Boussinesq equations constitute a dynamical system of great interest from the point of view of the bifurcation theory. It is complex enough to give rise to new or not well known spatio-temporal dynamics, but, since it is two-dimensional, it can still be deeply explored from numerical simulations for small aspect ratios. In this case, the number of coexistent flows is relatively small and low-dimensional dynamics may be expected. The nonlinear dynamics can be understood in terms of the bifurcation theory for systems of ordinary differential equations (ODEs). In this sense, the results presented in this paper also concern other problems that are equivariant

2000 *Mathematics Subject Classification.* Primary: 37M20, 65P30; Secondary: 76D05, 76E06.
Key words and phrases. Amplitude equations, symmetric periodic orbits, thermal convection.

under the same symmetry group ($\mathbb{O}(2)$). Such is the case of the dynamics that arises on a thin smectic-A liquid crystal film suspended in a small annulus, with an electric field applied in the radial direction [5], or of Rayleigh-Bénard convection [3, 7].

We develop a perturbation method to build and analyze the amplitude equations near a codimension-two bifurcation of a group orbit of symmetric time periodic solutions. They are direction reversing traveling waves, which drift back and forth in the angular direction without net drift [8]. Due to the rotation invariance of the problem, the group orbit is a circle. The codimension-two point was detected by integrating the full PDE system, and the numerical results indicate that the bifurcated flows keep some spatio-temporal symmetries, which consequently prevent net azimuthal drift. This dynamical behavior may seem anomalous in the context of known bifurcation theory, and requires a theoretical explanation.

One of the techniques usually employed to study theoretically the dynamics and bifurcations of symmetric periodic orbits consists of constructing return maps, in order to describe the trajectories avoiding the time dependence of the periodic orbits [17]. Other authors adopt a more formal approach and study the problem in the context of equivariant bifurcation theory [10, 16, 11]. Probably, the method used in [2, p.135, VI.1] for ribbon solutions in the Taylor-Couette problem is the most closely related to the method developed here. However, the time evolution for the ribbon solutions is trivial because they are azimuthal rotating waves, and the coefficients of the amplitude equations are not computed.

We propose a new approach to account for the nonlinear dependence of the period of the orbits, which can be thought as a generalization of the Lindstedt-Poincaré technique of ODEs to PDEs. It is a semi-analytical classical technique of relatively easy application to systems with quadratic nonlinearities. This technique allows to calculate (the coefficients of) the amplitude equations that describe the dynamics on the center manifold associated with bifurcation points, including spatial symmetry-breaking transitions. Equivariant bifurcation theory alone does not provide the numerical values of the coefficients, and return maps are not directly known in PDE systems, which is an additional strong difficulty when trying to calculate amplitude equations using this approach. In this paper, the symmetry properties of the eigenfunctions obtained in the numerical linear stability analysis of a circle of stable $\mathbb{D}_4$-symmetric periodic orbits u_s, found for radius ratios $0.3 < \eta < 0.35$, are used to derive the amplitude equations, to anticipate the appropriate expansion of u_s, and to simplify the recursive system of nonhomogeneous equations that involve the coefficients. These equations exhibit T-periodic solutions if and only if their forcing terms are orthogonal to the five linearly independent periodic orbits of the adjoint problem. Weakly nonlinear Floquet analysis of PDEs is also used in [18], [15] for the study of pattern formation in weakly damped Faraday waves, but in this case the problem is self-adjoint and the basic solution analytically known.

The paper is organized as follows. After the introduction and the statement of the problem in Sec. 2, Sec. 3 describes the linear stability analysis of the PDEs, and the symmetries of the eigenfunctions at the multi-critical bifurcation point. Secs. 4 and 5 deal with the amplitude equations and with the system of linear partial differential equations that determine the coefficients through the appropriate solvability conditions. The latter are derived in an appendix, where the formulation and resolution of the adjoint problem is also given. The amplitude equations are analyzed in Sec. 6, and the final conclusions are contained in Sec. 7.

2. **Thermal convection in a circular annulus.** Let us consider Boussinesq thermal convection in a two-dimensional annulus of inner and outer radii R_i and $R_o = R_i + d$, heated from inside. The problem is governed by mass conservation, Navier-Stokes and energy equations,

$$\begin{aligned} \nabla \cdot \mathbf{v} &= 0, & (1)\\ (\partial_t + \mathbf{v}\cdot\nabla)\mathbf{v} &= -\rho_i^{-1}\nabla p + \nu\nabla^2\mathbf{v} - \alpha\mathbf{g}(T - T_i), & (2)\\ (\partial_t + \mathbf{v}\cdot\nabla)T &= \kappa\nabla^2 T, & (3) \end{aligned}$$

respectively, where $\mathbf{v}$ is the velocity field, T the temperature, ρ_i the density at T_i, p the deviation of the pressure from the hydrostatic pressure, $\mathbf{g} = -g\hat{\mathbf{e}}_r$ the radial gravity vector, α the thermal expansion coefficient, ν the kinematic viscosity, and κ the thermal diffusivity of the fluid. Non-slip and perfectly conducting boundary conditions are taken, namely $\mathbf{v} = 0$, and $T = T_i$ and $T = T_o$ at R_i and R_o, respectively.

By taking $\Delta T = T_i - T_o$, d, and d^2/κ as temperature, length, and time units, respectively, the three non-dimensional parameters that appear in the equations are the radius ratio, $\eta = R_i/R_o$, the Prandtl number, $\sigma = \nu/\kappa$, and the Rayleigh number, $Ra = \alpha\Delta\mathrm{T}gd^3/\kappa\nu$. With this scaling, the non-dimensional inner and outer radii are $R_i = \eta/(1-\eta)$ and $R_o = 1/(1-\eta)$, and the non-dimensional fields are $\mathbf{u} = (d/\kappa)\mathbf{v}$, and $\mathcal{T} = T/\Delta T$.

In order to eliminate the pressure, the velocity $\mathbf{u}$ is written as $\mathbf{u} = f\hat{\mathbf{e}}_\theta + \nabla\times(\psi\hat{\mathbf{e}}_z)$, where $\hat{\mathbf{e}}_z$ is the unit vector perpendicular to the plane of the annulus. Then, the stream function

$$\Psi(t,r,\theta) = \psi(t,r,\theta) - \int_{R_i}^{r} f(t,r)dr \tag{4}$$

verifies $\mathbf{u} = \nabla\times(\Psi\hat{\mathbf{e}}_z)$, $f(t,r) = P_\theta u_\theta(t,r,\theta)$, and $P_\theta\psi(t,r,\theta) = 0$, where

$$P_\theta g(t,r,\theta) = \frac{1}{2\pi}\int_0^{2\pi} g(t,r,\theta)d\theta$$

is the azimuthal average operator. Note that the azimuthal mean flow f is needed if the azimuthal average of ψ is imposed to be zero by using homogeneous boundary conditions, which are convenient in numerical computations.

The equations for f and ψ are the azimuthal average of the azimuthal component of the Navier-Stokes equation, and the z component of its curl, respectively. The energy equation is written for the perturbation of the conductive state $\Theta = \mathcal{T} - \mathcal{T}_c$, the conductive state being $\mathbf{u} = 0$, $\mathcal{T}_c(r) = \mathcal{T}_i + \ln(r/R_i)/\ln\eta$. Then,

$$\begin{pmatrix} I & 0 & 0\\ 0 & I & 0\\ 0 & 0 & \Delta \end{pmatrix}\partial_t \begin{pmatrix} f\\ \Theta\\ \psi \end{pmatrix} = \begin{pmatrix} \sigma\tilde{\Delta} & 0 & 0\\ 0 & \Delta & -(r^2\ln\eta)^{-1}\partial_\theta\\ 0 & \sigma r^{-1}Ra\ \partial_\theta & \sigma\Delta\Delta \end{pmatrix}\begin{pmatrix} f\\ \Theta\\ \psi \end{pmatrix} + \begin{pmatrix} P_\theta\left[\Delta\psi\partial_\theta\psi\right]/r\\ J(\psi,\Theta) - f\partial_\theta\Theta/r\\ (1-P_\theta)J(\psi,\Delta\psi) + \tilde{\Delta}f\partial_\theta\psi/r - f\partial_\theta\Delta\psi/r \end{pmatrix}, \tag{5}$$

where $\Delta = (\partial_r + 1/r)\partial_r + (1/r^2)\partial^2_{\theta\theta}$, $\tilde{\Delta} = \partial_r(\partial_r + 1/r)$, and $J(h,g) = (\partial_r h\partial_\theta g - \partial_r g\partial_\theta h)/r$. With this formulation, the no-slip boundary conditions for the velocity field, and the conditions for the temperature perturbation at the boundaries are

$$f = \psi = \partial_r\psi = \Theta = 0 \quad \text{at } r = R_o, R_i. \tag{6}$$

See [14] for details. A simple inspection reveals that the system is $O(2)$-equivariant, $O(2)$ being generated by arbitrary rotations and reflections with respect to diameters, i.e., the actions

$$\begin{array}{ll} \theta \to \theta + \theta_0, & u \to u \\ \theta \to 2\theta_0 - \theta, & u \to \zeta u, \end{array} \tag{7}$$

with $u = (f, \Theta, \psi)$ and $\zeta u = (-f, \Theta, -\psi)$, leave the system invariant. The equations are autonomous, and so invariant under arbitrary time translations $t \to t + t_0$.

3. **Symmetric periodic orbits and their stability.** The conductive steady state is an $O(2)$ invariant solution of the system for any Ra and σ values. Below the critical Rayleigh number for the onset of thermal convection, heat is transported by conduction. When Ra is increased, keeping $\sigma = 0.025$ and η near 0.3, the conductive steady state suffers successive steady bifurcations, which break its invariance under arbitrary rotations. The new nonaxisymmetric steady solutions have consecutive azimuthal wavenumbers $n = 3, 2, 4$, etc., but maintain the reflection symmetry ρ_{θ_k}, with respect to appropriate diameters $\theta_k = \theta_0 + k\pi/n$, and the invariance under $2k\pi/n$ rotations, $\tilde{\sigma}_{2k\pi/n}$, with $k = 0, 1, \ldots, n-1$. The angular phase θ_0 is fixed by the initial conditions. The discrete spatial symmetry group of these steady solutions is $\mathbb{D}_n$, generated by the $2\pi/n$ rotation, and the reflection through $\theta_1 = \theta_0 + \pi/n$, i. e.,

$$\begin{array}{lll} \rho_{2\pi/n}: & \theta \to \theta + 2\pi/n, & u \to u, \\ \tilde{\sigma}_{\theta_1}: & \theta \to 2\theta_1 - \theta, & u \to \zeta u. \end{array}$$

Their spatio-temporal symmetry group is $\mathbb{D}_n \times \mathbb{R}$, where $\mathbb{R}$ is the time translations group.

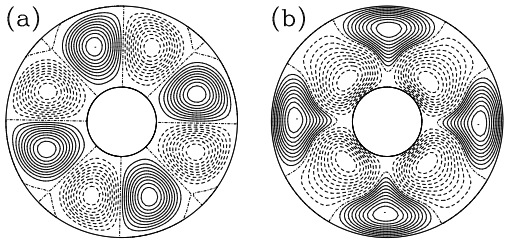

FIGURE 1. Stable $n = 4$ steady solution at $Ra = 6300$, and $\eta = 0.3$.

Bifurcations from the conductive state are symmetry-breaking steady-state bifurcations in which multiplicity two eigenvalues cross the imaginary axis and generate a circle of solutions. All the steady states above described, except for the branch with azimuthal wavenumber $n = 3$ are, initially, unstable. However, the branch with azimuthal wavenumber $n = 4$ stabilizes at higher Ra values, after all positive eigenvalues have crossed back the imaginary axis. Fig. 1 shows the spatial symmetries of a stable steady solution on this branch at $Ra = 6300$, and $\eta = 0.3$. The stream function, $\Psi(t, r, \theta)$, is plotted on the left. Solid and dashed lines indicate, respectively, anti-clockwise and clockwise vortices. The temperature perturbation, $\Theta(t, r, \theta)$, is plotted on the right. Solid and dashed lines correspond, respectively, to higher and lower temperatures than that of the conductive state. This convention will be kept along the paper. All the contour plots of the paper have azimuthal phase $\theta_0 = 0$.

By increasing Ra further, the steady $n = 4$ branch loses stability in a Hopf bifurcation, which yields a new circle of stable time periodic orbits, u_s, plotted as the lower horizontal line in the bifurcation diagrams of Figs. 2 and 3 (see [12] for further details on the sequence of bifurcations), and is labeled with $n = 4$ because u_s keeps the $\pi/2$-rotational symmetry of the steady state. The bifurcation breaks the (purely spatial) reflection symmetry of the steady solutions, but preserves a spatio-temporal reflection symmetry. Thus the spatio-temporal isotropy group of u_s (see Fig.4) is $\mathbb{D}_4$, generated by

$$\begin{aligned} \rho_{\pi/2} &: && \theta \to \theta + \pi/2, \quad u_s \to u_s, \\ \sigma_{\theta_1} &: \quad t \to t + T/2, && \theta \to 2\theta_1 - \theta, \quad u_s \to \zeta u_s, \end{aligned}$$

where T is the period of u_s, and $\theta_1 = \theta_0 + \pi/4$. Physically, these are direction reversing traveling waves without net azimuthal drift. From now on, we shall focus on this branch of symmetric time periodic orbits, which will be referred to as the *basic branch*.

The symmetric time periodic solutions, u, obtained for $\eta = 0.32$ and 0.35 are shown in figs. 2 and 3, respectively, where the norm $\|u - u_s\|_{L_2(\Omega)}$ (associated to the inner product defined in eq. (40) below) is plotted versus Ra. At every point of the diagram, u and u_s are calculated by using the Poincaré map obtained upon intersection of the orbits with the hyperplane defined such that the net azimuthal mass flow

$$\overline{f}(t) = \frac{1}{R_o - R_i} \int_{R_i}^{R_o} f(t, r)\, dr$$

vanishes. Newton-Krylov continuation of periodic orbits [19] is used, with Ra as the continuation parameter. The fields Θ and ψ are expanded in Fourier series in the azimuthal direction, and collocation for their coefficients and for f is employed in a radial mesh of Gauss-Lobatto points.

Solutions related by the symmetries of the system, (7), are projected onto the same point of the diagrams, and stable/unstable solutions are plotted with solid/dashed lines. This convention will be kept along the paper. The change of line style in the middle of branch (i) in Fig. 3, corresponds to a real $\mu = +1$ bifurcation, which breaks the last spatio-temporal symmetry of the periodic orbit, and so produces a branch of azimuthally drifting quasi-periodic orbits (not shown in Fig. 3). In the remaining bifurcation points some spatio-temporal reflection symmetries are preserved, and thus lead to bifurcated branches that exhibit no net azimuthal drift. Their stability is generally studied computing the Floquet multipliers (FM) with an Arnoldi method. If it is required due to multiplicities in the spectrum, a more expensive subspace iteration method is used.

At any value of Ra, the spectrum of the linearized problem around any periodic solution, u, has two marginal $\mu = +1$ FMs due to invariance under rotation and time translation with eigenfunctions

$$U_4 = \partial_\theta u, \qquad U_5 = \partial_t u.$$

When $\eta = 0.32$ (Fig. 2), the first pitchfork bifurcation on the $n = 4$ branch at $Ra = 10557$ is an azimuthal subharmonic (the $(\pi/2)$-azimuthal period is doubled) instability. It preserves the invariance under a π rotation, and in consequence is labeled as $n = 2$ (the label (ii) is also used for comparison with the final results). The second instability at $Ra = 10961$ is associated with a double $\mu = +1$ FM, and breaks all spatial symmetries. Thus it yields two different bifurcated branches (i) and (iii)(a), not related by the symmetries of the system. Instead, when $\eta =$

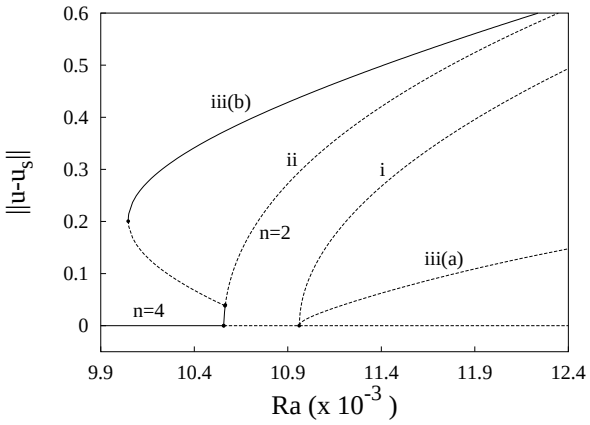

FIGURE 2. Bifurcation diagram of symmetric periodic orbits for $\eta = 0.32$.

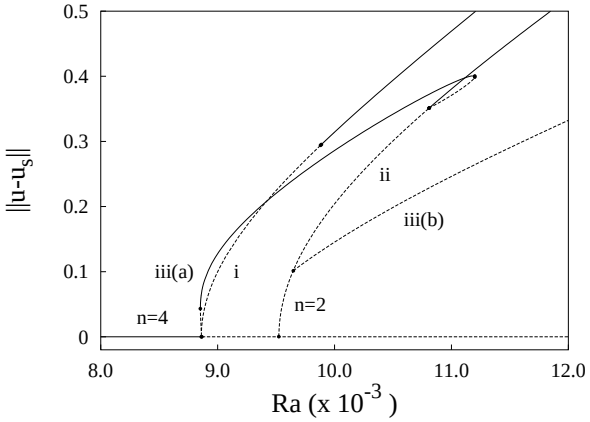

FIGURE 3. Bifurcation diagram of symmetric periodic orbits for $\eta = 0.35$.

0.35 (Fig. 3), the first instability at $Ra = 8860$ is the one that breaks all the spatial symmetries and gives rise to branches (i) and (iii)(a), the latter being now subcritical. This implies that the order in which these two bifurcations occur as Ra is increased is reversed as η moves between these two values. Thus, both bifurcation points must coalesce at some intermediate value of η. We are interested in studying this codimension-two point, obtained numerically at the critical radius ratio $\eta_c = 0.3255$ and critical Rayleigh number $Ra_c = 10385$. At this point the double FM (forced by the symmetries), and the spatial subharmonic pitchfork bifurcations of time periodic orbits collapse in a triple $\mu = +1$ bifurcation (plus the other two FM with eigenfunctions U_4, U_5 defined above). Since the solutions that bifurcate from the basic branch still preserve some spatio-temporal reflection symmetries, all the branches of time periodic solutions plotted in figs.2 and 3 at $\eta = 0.32$ and 0.35 correspond to solutions with no net drift. Now, we are interested in elucidating

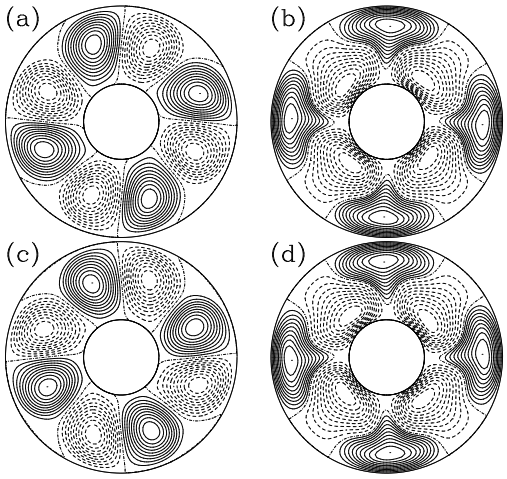

FIGURE 4. From left to right, (a), (b) instantaneous streamlines and temperature perturbation, respectively, for $u_s(0)$, and (c), (d) for $u_s(T/2)$. $Ra_c = 10385$, $\eta_c = 0.3255$.

whether mode interactions near the codimension-two point can break the spatio-temporal reflection symmetry and trigger net-drifting instabilities [4].

Let U_i, with $i = 1, \ldots, 5$, be the eigenfunctions associated to the quintuple $\mu = +1$ FM. If U_1, U_2 correspond to the double FM, they can be chosen such that $U_1(t, r, \theta) = -U_2(t, r, \theta + \pi/2)$ (see the first and third rows of Fig. 5). Both break the spatial symmetries of the basic solution, but each of them retain one spatio-temporal symmetry. Consequently, the symmetry groups of U_1 and U_2 are both $\mathbb{Z}_2$, generated by $\sigma_{\pi/2}$ and σ_0, respectively.

The eigenfunction U_3, shown in Fig. 6, breaks the $\pi/2$ rotational invariance, but maintains the invariance by a π rotation, and under spatio-temporal reflections by $\theta_1 = \pi/4$ and $\theta_3 = 3\pi/4$. Its symmetry group is $\mathbb{Z}_2 \times \mathbb{Z}_2$, generated by ρ_π and $\sigma_{\pi/4}$.

The eigenfunction $U_4 = \partial_\theta u_s$, shown in Fig. 7, maintains the $\pi/2$ rotational invariance, but changes the spatio-temporal symmetry because the azimuthal derivative introduces a change of sign. Its symmetry group is $\mathbb{Z}_4$ generated for instance by $\rho_{\pi/4}$. In addition, $U_5 = \partial_t u_s$ has the same symmetries as u_s (Fig. 8). Therefore, its symmetry group is $\mathbb{D}_4$ (see also [13]).

In order to anticipate the form of the amplitude equations, the spatial $\pi/2$ rotation and two spatio-temporal reflections by the diameters $\theta_1 = 0$ and $\theta_2 = \pi/2$ are considered, namely

$$\begin{array}{rccc} \rho_{\pi/2}: & & \theta \to \theta + \pi/2, & u_s \to u_s, \\ \sigma_0: & t \to t + T/2, & \theta \to -\theta, & u_s \to \zeta u_s, \\ \sigma_{\pi/2}: & t \to t + T/2, & \theta \to \pi - \theta, & u_s \to \zeta u_s, \end{array}$$

even though these are not independent, since $\sigma_{\pi/2} = \rho_{\pi/2}^2 \circ \sigma_0$.

4. **Symmetries of the eigenfunctions: Amplitude equations.** As indicated above, we could expect that the system exhibits drift instabilities (yielding rigid-like rotations around the origin) when the spatio-temporal reflection symmetries are broken. Then, near the codimension-two point, the rotation would be quite slow

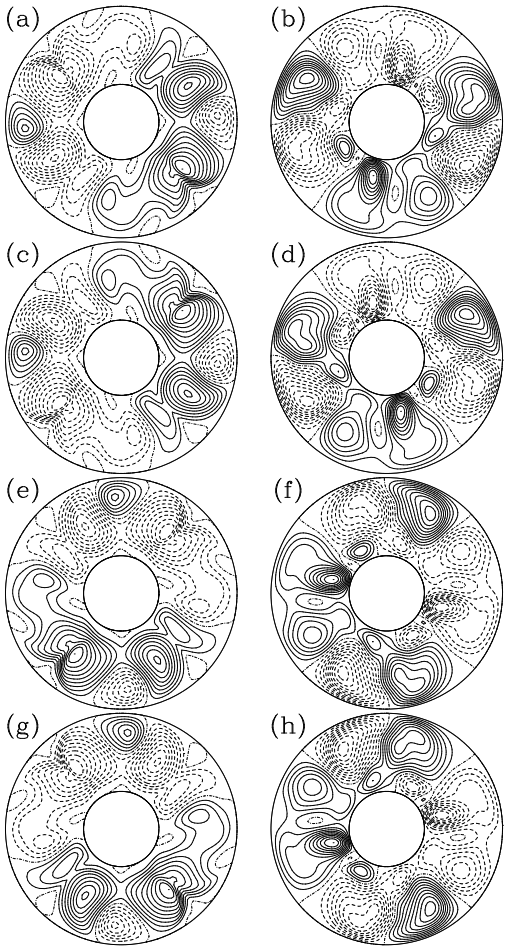

FIGURE 5. From left to right, (a), (b) instantaneous streamlines and temperature perturbation, respectively, for $U_1(0)$, (c), (d) for $U_1(T/2)$, (e), (f) for $U_2(0)$, and (g), (h) for $U_2(T/2)$. $Ra_c = 10385$, $\eta_c = 0.3255$.

and would involve the U_4-eigenmode associated with the invariance under rotations. As usually [4], a convenient weakly nonlinear description of these rotating solutions requires to use a rotating frame of reference with $\theta = \varphi(t)$, where the possibly non-constant (slow) azimuthal phase shift φ must be determined as a part of the solution. Similarly, because of the invariance under time translations we introduce a slow, time dependent temporal phase ϕ, which must also be determined as a part of the solution. The shifts φ and ϕ are associated with the U_4 and U_5 eigenmodes, respectively. Thus, near the multi-critical point the solution can be written as

$$u(t, r, \theta) = u_s(\tau, r, \theta - \varphi(\tilde{t})) + \sum_{j=1}^{3} A_j(\tilde{t}) U_j(\tau, r, \theta - \varphi(\tilde{t})) + \cdots , \tag{8}$$

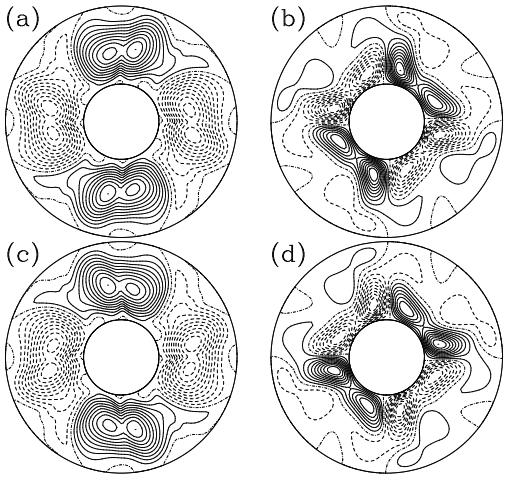

FIGURE 6. From left to right, (a), (b) instantaneous streamlines and temperature perturbation, respectively, for $U_3(0)$, and (c), (d) for $U_3(T/2)$. $Ra_c = 10385$, $\eta_c = 0.3255$.

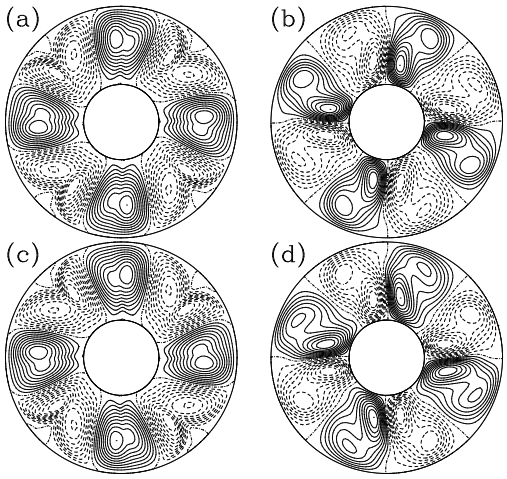

FIGURE 7. From left to right, (a), (b) instantaneous streamlines, and temperature perturbation, respectively, for $U_4(0)$, and (c), (d) for $U_4(T/2)$. $Ra_c = 10385$, $\eta_c = 0.3255$.

where τ and $\tilde{t}$ are a fast and a slow time variables, related to the original time variable as

$$\tau = t - \phi(t), \quad \tilde{t} = t. \tag{9}$$

The amplitudes A_j are real because the eigenfunctions U_j are real. In order to make the analysis below more flexible, we are not scaling the slow time variable $\tilde{t}$. The fact that this variable is slow is imposed requiring that both the amplitudes and the phase shifts depend weakly on time, namely

$$|\dot{A}_j| \ll |A_j| \ll 1 \text{ for } j = 1, 2, 3, \quad |\dot{\varphi}| \ll 1, \quad |\dot{\phi}| \ll 1, \tag{10}$$

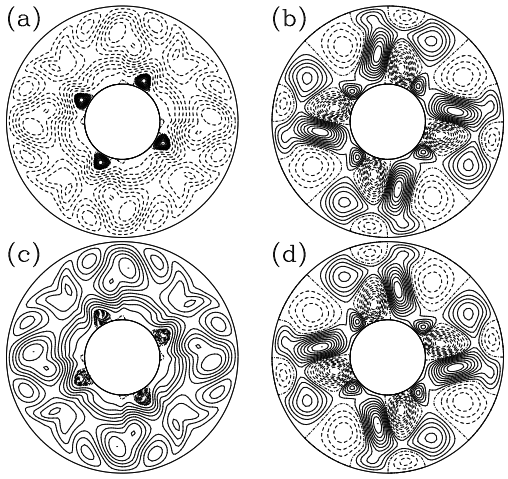

FIGURE 8. From left to right, (a), (b) instantaneous streamlines, and temperature perturbation, respectively, for $U_5(0)$, and (c), (d) for $U_5(T/2)$. $Ra_c = 10385$, $\eta_c = 0.3255$.

where the dot means d/dt, and we are also imposing that the real amplitudes be small (as required by the weakly-nonlinear level of our analysis), namely that the solution be close to a (conveniently rotated and translated in time) base solution.

The structure of the amplitude equations is restricted by the symmetries of the eigenfunctions at the codimension-two bifurcation point. These symmetries can be extracted from figures (4-6), to be

$$\tau \to \tau + T/2, \quad \theta \to -\theta, \quad \varphi \to -\varphi \implies \begin{cases} u_s \to \zeta u_s, & U_1 \to -\zeta U_1, \\ U_2 \to \zeta U_2, & U_3 \to -\zeta U_3, \end{cases}$$

$$\tau \to \tau + T/2, \quad \theta \to \pi - \theta, \quad \varphi \to \pi - \varphi \implies \begin{cases} u_s \to \zeta u_s, & U_1 \to \zeta U_1, \\ U_2 \to -\zeta U_2, & U_3 \to -\zeta U_3, \end{cases}$$

$$\theta \to \theta + \pi/2, \quad \varphi \to \varphi + \pi/2 \implies \begin{cases} u_s \to u_s, & U_1 \to -U_2, \\ U_2 \to U_1, & U_3 \to -U_3. \end{cases}$$

These lead to the following symmetries in terms of the amplitudes A_j, the phase shift φ, and the time shift ϕ transformations

$$\begin{array}{llll} \varphi \to -\varphi, & A_1 \to -A_1, & A_3 \to -A_3, & \\ \varphi \to \pi - \varphi, & A_2 \to -A_2, & A_3 \to -A_3, & \\ \varphi \to \varphi + \pi/2, & A_1 \to -A_2, & A_2 \to A_1, & A_3 \to -A_3. \end{array} \tag{11}$$

Up to third order, the most general equations that are invariant under the above symmetries are of the form

$$\dot{A}_1 = (\alpha_1\varepsilon_1 + \alpha_3\varepsilon_2)A_1 + \beta_1 A_2 A_3 + (\gamma_1 A_1^2 + \gamma_2 A_2^2 + \gamma_3 A_3^2)A_1 \tag{12}$$

$$\dot{A}_2 = (\alpha_1\varepsilon_1 + \alpha_3\varepsilon_2)A_2 + \beta_1 A_1 A_3 + (\gamma_1 A_2^2 + \gamma_2 A_1^2 + \gamma_3 A_3^2)A_2 \tag{13}$$

$$\dot{A}_3 = (\alpha_2\varepsilon_1 + \alpha_4\varepsilon_2)A_3 + \beta_2 A_1 A_2 + [\gamma_4(A_1^2 + A_2^2) + \gamma_5 A_3^2]A_3 \tag{14}$$

$$\dot{\varphi} = \delta(A_1^2 - A_2^2)A_3, \tag{15}$$

$$\dot{\phi} = -\nu_1\varepsilon_1 - \nu_2\varepsilon_2 + \xi_1(A_1^2 + A_2^2) + \xi_2 A_3^2. \tag{16}$$

The unfolding parameters, $\varepsilon_1 = (Ra - Ra_c)/Ra_c$, and $\varepsilon_2 = \eta - \eta_c$ are small, namely

$$|\varepsilon_1| \ll 1, \quad |\varepsilon_2| \ll 1, \tag{17}$$

and the coefficients ν_1, α_1, α_2, β_1, β_2, $\gamma_1, \ldots, \gamma_5$, δ, ξ_1, and ξ_2 are all $\mathcal{O}(1)$ in the limit (17), and are determined through appropriate solvability conditions, which are considered below. The coefficients ν_2, α_3 and α_4 are obtained from the slopes of the plots in figures 9(b) and (d), resulting from the linear stability analysis.

Note that the amplitude equations (12)-(14) are decoupled from (15)-(16), and that the fourth equation gives the slow drift velocity of the pattern $\dot{\varphi}$, which vanishes identically in the invariant manifolds $A_1 = \pm A_2$ and $A_3 = 0$, but is generically nonzero outside these manifolds, and can lead to a slow net drift (recall that an additional fast, instantaneous drift of the pattern, with no net drift, was already present in the basic periodic solution).

5. **Determination of the coefficients of the amplitude equations.** The coefficients of the equations (12)-(16) are determined numerically by perturbing the solution u, and applying solvability conditions. For the sake of clarity, we only consider at the moment perturbations in the Rayleigh number, which only appears in the linear part of the right hand side of the equations (5). Perturbations in η instead will be avoided at this stage setting $\varepsilon_2 = 0$ (and added a posteriori, using fig.9), because they affect both the spatial domain and nonlinear terms in equations (5), and thus would lead to fairly involved perturbed equations.

At $\varepsilon_2 = 0$ (namely, $\eta = \eta_c$), the system (5) is rewritten as

$$\mathcal{L}_0 \partial_t u = \mathcal{L}_1 u + \varepsilon_1 \mathcal{L}_2 u + \mathcal{B}(u, u), \tag{18}$$

where $u = (f, \Theta, \psi)$, $\mathcal{L}_0$ denotes the linear operator appearing in the left hand side of eq. (5), while the linear operator appearing in the right hand side has been split into two parts because of its linear dependence on $Ra = Ra_c(1 + \varepsilon_1)$. The (non-symmetric) bilinear operator $\mathcal{B}$ results from convective terms, and is independent of Ra. The boundary conditions (6) are (implicitly) imposed in the domain of the linear operators; note that this implies that $\mathcal{L}_0$ admits a bounded inverse.

Since we have been able to anticipate the amplitude equations (12)-(16), we can also anticipate the appropriate expansion in the solution u. The amplitude equations contain terms that are not of the same order, and thus there are several distinguished limits (namely, several relations between the small parameter ε_1, the small amplitudes, and the large slow temporal scale in which the amplitudes evolve). In order to avoid restricting the analysis to a particular distinguished limit, we consider ε_1 and the amplitudes A_j as independent small quantities, and seek a series expansion of the solution in powers of these quantities, up to the appropriate order. The basic solution u_s and the eigenfunctions U_j must be expanded in powers of ε_1, as

$$\begin{aligned} u_s &= u_s^0 + \varepsilon_1 u_s^1 + \cdots \\ U_j &= U_j^0 + \varepsilon_1 U_j^1 + \cdots \quad \text{for } j = 1, \ldots, 3, \end{aligned}$$

The expansions (8) are rewritten to include higher order terms, as

$$u = u_s^0 + \varepsilon_1 u_s^1 + \sum_{j=1}^{3} A_j (U_j^0 + \varepsilon_1 U_j^1) + \sum_{\substack{k,l=1 \\ k \le l}}^{3} A_k A_l U_{kl}^1 + \sum_{j=1}^{3} A_j \sum_{k=1}^{3} A_k^2 U_{jk}^2 + \ldots, \tag{19}$$

where all the functions u_s^m, U_j^m, and U_{jk}^m depend on $(\tau, r, \theta - \varphi)$, and A_j and φ depend weakly on t (see (10)), with the fast and slow time variables, τ and $\tilde{t}$ defined in (9). Note that this means that the time derivative of u in eq. (18) must be calculated as

$$\partial_t = (1 - \dot{\phi})\partial_\tau - \dot{\varphi}\partial_\theta + \partial_{\tilde{t}},$$

and that $U_{kl}^1 = U_{lk}^1$. Also, we are neglecting ε_1-perturbations of U_{kl}^1 and U_{jk}^2, which are not needed below, and only those third order terms that contribute to the amplitude equations are displayed. For convenience, we rewrite the amplitude equations (12)-(16) as

$$\dot{A}_j(t) = \tilde{\alpha}_j \varepsilon_1 A_j + \sum_{\substack{k,l=1 \\ k \le l}}^{3} \tilde{\beta}_{jkl} A_k A_l + A_j \sum_{k=1}^{3} \tilde{\gamma}_{jk} A_k^2, \quad j = 1, 2, 3 \tag{20}$$

$$\dot{\varphi}(t) = \sum_{\substack{j,k=1 \\ j \neq k}}^{3} \tilde{\delta}_{jk} A_j A_k^2, \tag{21}$$

$$\dot{\phi}(t) = -\tilde{\nu}_1 \varepsilon_1 + \sum_{j=1}^{3} \tilde{\xi}_j A_j^2. \tag{22}$$

Comparison with (12)-(16) shows that

$$\begin{gathered} \tilde{\nu}_1 = \nu_1, \quad \tilde{\alpha}_1 = \tilde{\alpha}_2 = \alpha_1, \quad \tilde{\alpha}_3 = \alpha_2, \quad \tilde{\beta}_{123} = \tilde{\beta}_{213} = \beta_1, \quad \tilde{\beta}_{312} = \beta_2, \\ \tilde{\gamma}_{11} = \tilde{\gamma}_{22} = \gamma_1, \tilde{\gamma}_{12} = \tilde{\gamma}_{21} = \gamma_2, \quad \tilde{\gamma}_{13} = \tilde{\gamma}_{23} = \gamma_3, \quad \tilde{\gamma}_{31} = \tilde{\gamma}_{32} = \gamma_4, \\ \tilde{\gamma}_{33} = \gamma_5, \quad \tilde{\delta}_{31} = -\tilde{\delta}_{32} = \delta, \quad \tilde{\xi}_1 = \tilde{\xi}_2 = \xi_1, \quad \tilde{\xi}_3 = \xi_2, \end{gathered} \tag{23}$$

the remaining coefficients $\tilde{\beta}_{jkl}$, $\tilde{\gamma}_{jk}$, and $\tilde{\delta}_{jk}$ being zero.

Substituting the expansion (19) and the amplitude equations (20)-(22) into (18), and setting to zero the coefficient of each monomial in ε_1, A_1, A_2, and A_3, we obtain a recursive system of linear equations that are nonhomogeneous versions of the equation that gives the eigenfunctions U_j^0 for $j = 1, \ldots, 5$, which is eq. (25) below. Since this homogeneous equation is singular, namely it exhibits nontrivial T-periodic solutions, when a forcing term is added the resulting equation does possess T-periodic solutions only if the forcing term satisfies an appropriate solvability condition, which is obtained in the Appendix. This will determine the coefficients, $\tilde{\nu}_1$, $\tilde{\alpha}_j$, $\tilde{\beta}_{jkl}$, $\tilde{\gamma}_{jk}$, $\tilde{\delta}_{jk}$, and $\tilde{\xi}_j$ in the amplitude equations (20)-(21). *At leading order*, we obtain

$$\mathcal{L}_0 \partial_\tau u_s^0 = \mathcal{L}_1 u_s^0 + \mathcal{B}(u_s^0, u_s^0),$$

which is the equation verified by the unperturbed, basic solution u_s^0. *At order* $\mathcal{O}(\varepsilon_1)$, we get

$$\mathcal{L}_0 \partial_\tau u_s^1 = \mathcal{L}_1 u_s^1 + \mathcal{B}(u_s^0, u_s^1) + \mathcal{B}(u_s^1, u_s^0) + \mathcal{L}_2 u_s^0 - \tilde{\nu}_1 \mathcal{L}_0 \partial_\tau u_s^0, \tag{24}$$

which gives the ε_1-correction to the basic solution. By applying solvability conditions it provides $\tilde{\nu}_1$. *At order* $\mathcal{O}(A_j)$, the relevant equation is

$$\mathcal{L}_0 \partial_\tau U_j^0 = \mathcal{L}_1 U_j^0 + \mathcal{B}(u_s^0, U_j^0) + \mathcal{B}(U_j^0, u_s^0), \tag{25}$$

which is the equation verified by the unperturbed eigenfunctions. *At order* $\mathcal{O}(\varepsilon_1 A_j)$, the following equation results

$$\begin{aligned}\mathcal{L}_0\partial_\tau U_j^1 = {} & \mathcal{L}_1 U_j^1 + \mathcal{B}(u_s^0, U_j^1) + \mathcal{B}(U_j^1, u_s^0) + \mathcal{L}_2 U_j^0 + \mathcal{B}(u_s^1, U_j^0) + \mathcal{B}(U_j^0, u_s^1) \\ & - \tilde{\nu}_1 \mathcal{L}_0 \partial_\tau U_j^0 - \tilde{\alpha}_j \mathcal{L}_0 U_j^0.\end{aligned} \tag{26}$$

This equation provides both the ε_1-corrections of the eigenfunctions and (applying a solvability condition) the coefficients $\tilde{\alpha}_j$. *At order* $\mathcal{O}(A_k A_l)$, with $j \neq k$, we obtain

$$\begin{aligned}\mathcal{L}_0\partial_\tau U_{kl}^1 = {} & \mathcal{L}_1 U_{kl}^1 + \mathcal{B}(u_s^0, U_{kl}^1) + \mathcal{B}(U_{kl}^1, u_s^0) + \mathcal{B}(U_k^0, U_l^0) + \mathcal{B}(U_l^0, U_k^0) \\ & - \sum_{j=1}^{3} \tilde{\beta}_{jkl} \mathcal{L}_0 U_j^0,\end{aligned} \tag{27}$$

which provides the coefficients $\tilde{\beta}_{jkl}$, and the functions U_{kl}^1, with $k \neq l$. If instead $k = l$, then we have

$$\mathcal{L}_0\partial_\tau U_{kk}^1 = \mathcal{L}_1 U_{kk}^1 + \mathcal{B}(u_s^0, U_{kk}^1) + \mathcal{B}(U_{kk}^1, u_s^0) + \mathcal{B}(U_k^0, U_k^0) + \tilde{\xi}_k \mathcal{L}_0 \partial_\tau u_s^0, \tag{28}$$

which allows to calculate the functions U_{kk}^1 (recall that $\tilde{\beta}_{jkk} = 0$), and $\tilde{\xi}_k$. *At order* $\mathcal{O}(A_j A_k^2)$, with $j \neq k$, we obtain

$$\begin{aligned}\mathcal{L}_0\partial_\tau U_{jk}^2 = {} & \mathcal{L}_1 U_{jk}^2 + \mathcal{B}(u_s^0, U_{jk}^2) + \mathcal{B}(U_{jk}^2, u_s^0) + \mathcal{B}(U_{kk}^1, U_j^0) + \mathcal{B}(U_j^0, U_{kk}^1) \\ & + \mathcal{B}(U_{jk}^1, U_k^0) + \mathcal{B}(U_k^0, U_{jk}^1) - 2\sum_{l=1}^{3} \hat{\beta}_{ljk} \mathcal{L}_0 U_{kl}^1 - \tilde{\gamma}_{jk} \mathcal{L}_0 U_j^0 \\ & + \tilde{\delta}_{jk} \mathcal{L}_0 \partial_\theta u_s^0 + \tilde{\xi}_k \mathcal{L}_0 \partial_\tau U_j^0,\end{aligned} \tag{29}$$

where $\hat{\beta}_{ljk} = \tilde{\beta}_{ljk}/2$ if $j < k$, and $\hat{\beta}_{ljk} = \tilde{\beta}_{lkj}/2$ if $j > k$. This provides the coefficients $\tilde{\gamma}_{jk}$ and $\tilde{\delta}_{jk}$. If instead $j = k$, we obtain

$$\begin{aligned}\mathcal{L}_0\partial_\tau U_{jj}^2 = {} & \mathcal{L}_1 U_{jj}^2 + \mathcal{B}(u_s^0, U_{jj}^2) + \mathcal{B}(U_{jj}^2, u_s^0) + \mathcal{B}(U_{jj}^1, U_j^0) + \mathcal{B}(U_j^0, U_{jj}^1) \\ & - \tilde{\gamma}_{jj} \mathcal{L}_0 U_j^0.\end{aligned} \tag{30}$$

which provides the coefficients $\tilde{\gamma}_{jj}$ (recall that $\tilde{\delta}_{jj} = 0$).

This completes the derivation of the coefficients of the amplitude equations (20)-(22) or, invoking (23), the coefficients of (12)-(16). These are as given below, in (31). In addition, we have checked that the parity and symmetries of the functions u_s^1, U_j^1, and U_{jk}^1 $(j, k = 1, 2, 3)$, obtained in the computation of the constants are those expected from the recursive system of equations.

Looking at the perturbations (19), and at the linear approximations of the amplitude equations (20), it turns out that the FM associated with U_1 and U_3 (at $\varepsilon_2 = 0$) are $\mu_1 = \exp(\tilde{\alpha}_1 \varepsilon_1 T) \simeq 1 + \tilde{\alpha}_1 \varepsilon_1 T$ and $\mu_2 = \exp(\tilde{\alpha}_3 \varepsilon_1 T) \simeq 1 + \tilde{\alpha}_3 \varepsilon_1 T$. This provides an alternative, direct method to calculate $\tilde{\alpha}_1 = \alpha_1$ and $\tilde{\alpha}_3 = \alpha_2$ (see (23)). Similarly, α_3 and α_4 of equations (12)-(14) can be calculated through the ε_2-perturbations of the Floquet multipliers at $\varepsilon_1 = 0$, as $\mu_1 = \exp(\alpha_3 \varepsilon_2 T) \simeq 1 + \alpha_3 \varepsilon_2 T$ and $\mu_2 = \exp(\alpha_4 \varepsilon_2 T) \simeq 1 + \alpha_4 \varepsilon_2 T$. The slopes m_D of the double FM, m_S of the simple FM displayed in Fig. 9(a), and the period $T = 0.1395$ of u_s at $Ra_c = 10385$, give $\alpha_1 = m_D/T = 2.88$, $\alpha_2 = m_S/T = 1.26$. Those displayed in Fig. 9(b) give $\alpha_3 = m_D/T = 26.09$, and $\alpha_4 = m_S/T = 4.13$. Moreover, when $A_j = 0$, the plots of T versus ε_1 and ε_2 in Fig. 9(c, d) with the transformation $\tau = (1 + \nu_1 \varepsilon_1 + \nu_2 \varepsilon_2)t$ supply an estimate of $\tilde{\nu}_j = \nu_j = -m_{jT}/T$, for j=1 and 2. They give $\nu_1 = 0.556$,

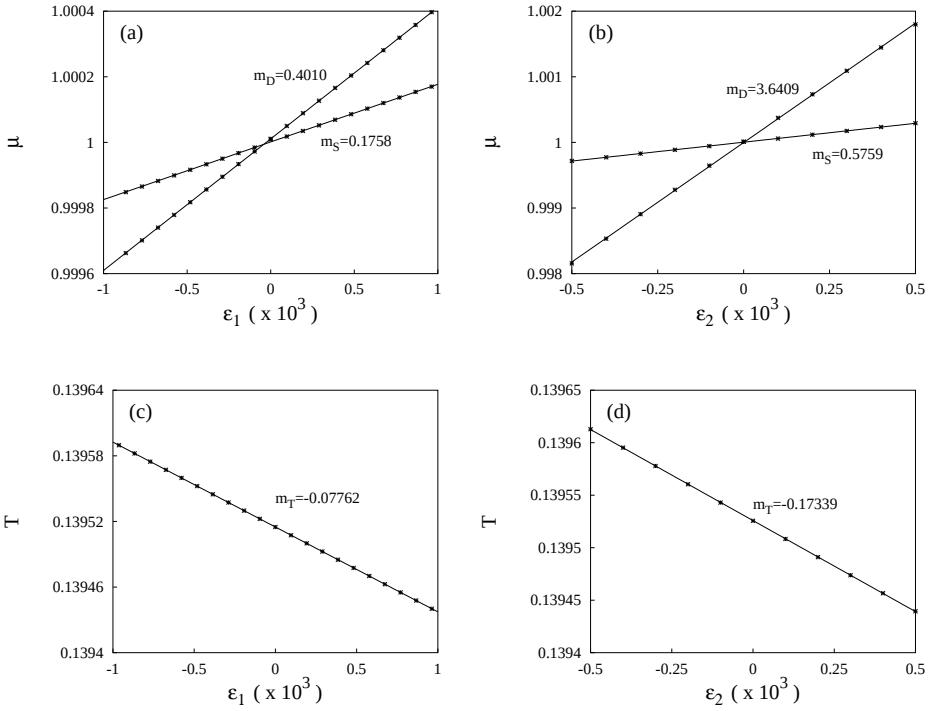

FIGURE 9. Linear dependence of the leading Floquet multipliers near the multi-critical point versus the unfolding parameters: a) ε_1, and (b) ε_2. Linear dependence of the period T, (c) on ε_1, and (d) on ε_2.

and $\nu_2 = 1.24$. The values of the coefficients ν_1, α_1 and α_2 agree very well with those calculated using the solvability conditions on eqs.(24) and (26).

Finally, we have all coefficients in eqs.(12)-(16), which are

$$\begin{gathered}\alpha_1 = 2.88, \quad \alpha_2 = 1.26, \quad \alpha_3 = 26.09, \quad \alpha_4 = 4.13, \quad \beta_1 = 0.805, \quad \beta_2 = 0.540, \\ \gamma_1 = -0.157, \quad \gamma_2 = -0.339, \quad \gamma_3 = -0.491, \quad \gamma_4 = -0.126, \quad \gamma_5 = -0.0519, \\ \delta = 0.576, \quad \xi_1 = 0.00217, \quad \xi_2 = 0.495, \quad \nu_1 = 0.560, \quad \nu_2 = 1.24.\end{gathered} \tag{31}$$

Note that because $\alpha_3 = 26.09$ is fairly large, the unfolding parameter ε_2 must be extremely small, such that $\alpha_3\varepsilon_2 \ll 1$ to get good results.

6. **Analysis of the amplitude equation.** Now we consider the amplitude equations (12)-(16), with the various coefficients as given in (31). The bifurcation diagram for fixed ε_2 and varying ε_1, such that $|\varepsilon_1| \ll 1$ and $|\varepsilon_2| \ll 1$ is topologically equivalent to that in Fig. 10 if $\varepsilon_2 < 0$, and to that in Fig. 11 if $\varepsilon_2 > 0$. In these figures, we are plotting

$$\|u - u_s\|_{L_2(\Omega)} \simeq \sqrt{a_1(A_1^2 + A_2^2) + a_3 A_3^2},$$

where, from (19), $u - u_s \simeq \sum_{j=1}^{3} A_j U_j^0$, the weights are $a_1 = \|U_1^0\|_{L_2(\Omega)} = \|U_2^0\|_{L_2(\Omega)}$ and $a_3 = \|U_3^0\|_{L_2(\Omega)}$, and mutual orthogonality of U_1^0, U_2^0, and U_3^0 is taken into

account. Also, numerical integration of the amplitude equations for various values of the parameters ε_1 and ε_2, and various initial conditions, show that for large time the solutions always converge to a steady state, which is of one of the following types:

i.- $(A_1, A_2, A_3) = (A, 0, 0)$ or $(0, A, 0)$, with A given by

$$\alpha_1\varepsilon_1 + \alpha_3\varepsilon_2 = -\gamma_1 A^2.$$

These branches bifurcate from the basic solution at $\varepsilon_1 = -\alpha_3\varepsilon_2/\alpha_1$, at a double-zero bifurcation.

ii.- $(A_1, A_2, A_3) = (0, 0, A_3)$, with A_3 given by

$$\alpha_2\varepsilon_1 + \alpha_4\varepsilon_2 = -\gamma_5 A_3^2, \tag{32}$$

which bifurcate from the basic solution at $\varepsilon_1 = -\alpha_4\varepsilon_2/\alpha_2$, in a pitchfork bifurcation.

iii.- $(A_1, A_2, A_3) = (A, \pm A, A_3)$, with $A \neq 0$ and $A_3 \neq 0$ given by

$$\begin{aligned} A^2 &= -\frac{\alpha_1\varepsilon_1 + \alpha_3\varepsilon_2 \pm \beta_1 A_3 + \gamma_3 A_3^2}{\gamma_1 + \gamma_2}, \\ \pm(\alpha_2\varepsilon_1 + \alpha_4\varepsilon_2)A_3 &- \frac{\alpha_1\varepsilon_1 + \alpha_3\varepsilon_2 \pm \beta_1 A_3 + \gamma_3 A_3^2}{\gamma_1 + \gamma_2}(\beta_2 \pm 2\gamma_4 A_3) \pm \gamma_5 A_3^3 = 0. \end{aligned} \tag{33}$$

This gives two bifurcated branches, namely (a) a primary bifurcation at $\varepsilon_1 = -\alpha_2\varepsilon_2/\alpha_1$, and (b) a secondary branch that bifurcates from the branch considered in (ii) at the point $(A_1, A_2, A_3) = (0, 0, A_3)$ such that (see (32), (33))

$$\alpha_1\varepsilon_1 + \alpha_3\varepsilon_2 \pm \beta_1 A_3 + \gamma_3 A_3^2 = \alpha_2\varepsilon_1 + \alpha_4\varepsilon_2 \pm \gamma_5 A_3^2 = 0. \tag{34}$$

The system (33) with $A_3 = 0$ or $A = 0$ recovers solutions (i) and (ii) respectively.

All steady states considered above are pure modes, and exhibit no slow drift ($\dot{\varphi} = 0$). In principle, the system could exhibit also mixed modes, such that $A_1 \neq A_2$ and $A_3 \neq 0$. This requires that the amplitudes be quite large as $\varepsilon_1 \to 0$ and $\varepsilon_2 \to 0$, which is outside the validity of the amplitude equations. By integrating the time dependent amplitude equations we have not found attractors at low amplitudes leading to quasi-periodic drifting dynamics.

Figures 10 and 11 display two bifurcation diagrams for $\varepsilon_2 = -0.0055$ ($\eta = 0.32$ as in Fig. 2) and 0.0045 ($\eta = 0.33$). All curves shown correspond to steady solutions of one of the above described types, and have been labeled accordingly. Because of the symmetries (11), each point of branches of types (i) and (iii) corresponds to four different steady states of the amplitude equations, and to two for points in case (ii). Note that, in both cases, the system exhibits, at least, one stable steady state.

In Fig. 10 the primary bifurcated branches from the basic solution ($A_1 = A_2 = A_3 = 0$) are found at $\varepsilon_1 = 0.0181$ and $\varepsilon_1 = 0.0498$. All of them are supercritical. The secondary bifurcated branch corresponds to steady states of type (iii)(b), with the bifurcation points given by (34).

Concerning Fig. 11, two primary branches bifurcate sub and supercritically at $\varepsilon_1 = -0.0407$, while the second primary bifurcation at $\varepsilon_1 = -0.0148$ is supercritical. Note that the upper branch of the first bifurcation terminates at a point of the primary branch starting at $\varepsilon_1 = -0.0148$. This end point and the starting point of the secondary branch satisfy (34). In any event, comparison of Figs. 10 and 11 confirms the interchange in order of the single and double bifurcations as

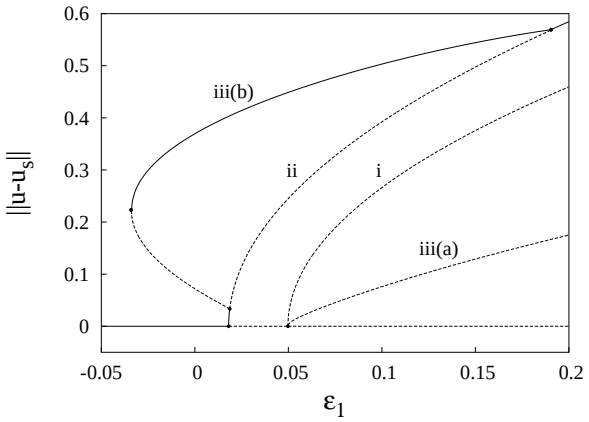

FIGURE 10. Stable (solid) and unstable (dashed) steady states of (12)-(14) for $\varepsilon_2 = -0.0055$.

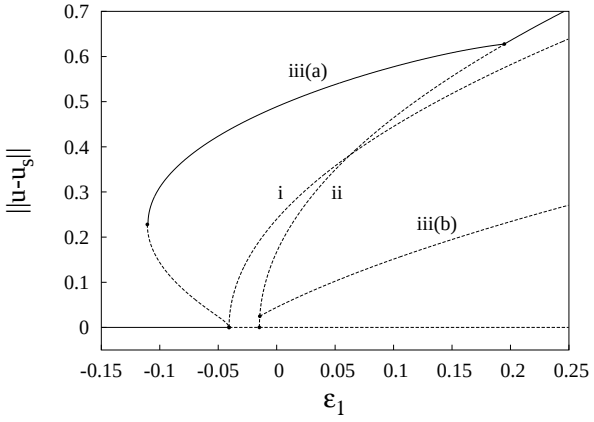

FIGURE 11. As in Fig. 10 for $\varepsilon_2 = +0.0045$.

ε_2 changes sign. It shows that $\mathbb{D}_4$-symmetric periodic orbits in $\mathbb{O}(2)$-equivariant systems have generically a double bifurcation point giving rise to two branches of symmetric periodic orbits with just one spatio-temporal reflection symmetry. One of these branches is supercritical for any ε_2 value, and the other is super/subcritical depending on whether $\varepsilon_2 < 0$ or $\varepsilon_2 > 0$, respectively. The simple pitchfork bifurcation is also supercritical for any ε_2 value, and the secondary bifurcation on this branch is also generic, being sub/supercritical for $\varepsilon_2 < 0$ or $\varepsilon_2 > 0$, respectively. As $\varepsilon_2 \to 0$ it moves to u_s. So, for any value of ε_2, only one of the branches emerging near $\varepsilon_1 = 0$ is subcritical (see also Fig. 12 corresponding to $\varepsilon_2 = 0$).

The next three figures show the comparison between the bifurcation diagrams corresponding to the initial PDE (thick lines) and the system of ODE (12)-(14) (thin lines) for three different values of ε_2. Figs. 2 and 10 have been superposed in Fig. 13, and Fig. 11 and the bifurcation diagram obtained from the PDE system for $\varepsilon_2 = +0.0045$ in Fig. 14. Both diagrams show that for small amplitudes,

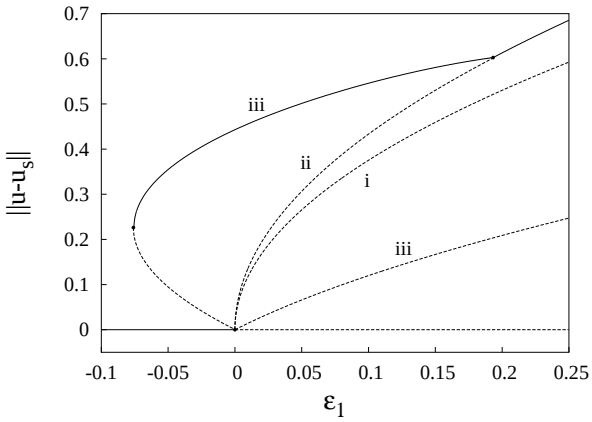

FIGURE 12. As in Fig. 10 for $\varepsilon_2 = 0$.

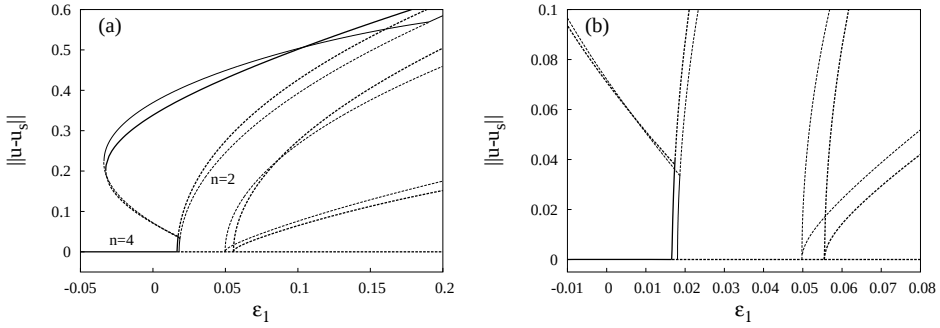

FIGURE 13. Superposition of Figs. 2 and 10 for $\varepsilon_2 = -0.0055$. (b) Detail of (a) for small amplitudes. The thick and thin lines correspond to the PDE and the ODE systems, respectively.

and $\varepsilon_2 = \eta - \eta_c$ small and constant, the system of ODEs reproduce quantitatively the bifurcations found in the PDEs, and at least the qualitative behavior and the stability of any branch, even at high amplitudes. The small differences in the bifurcation points of the $n = 4$ branch are due to the dependence of the eigenvalues on ε_1^2 and ε_2^2, which has not been taken into account. The larger differences in secondary bifurcations, especially in the turning (saddle-node) point in Fig. 14 are due to the neglected higher order nonlinear terms. Note that the good quantitative agreement is sometimes surprising since the involved values of $\|u - u_s\|$ (say, 0.5 in Fig. 13) cannot be considered small. If necessary, to correct the mismatch of Figs. 13 and Fig. 14, the second order terms could be added in the model a posteriori by extending Fig. 9 to higher ε_1, ε_2 values, and fitting a quadratic curve.

As anticipated at the end of last section, high ε_2 values are too large to get good quantitative comparison with the numerically obtained solution. This is illustrated in Fig. 15, which is a superposition of Fig. 3 ($\eta = 0.35$) with the corresponding diagram given by the amplitude equations for $\varepsilon_2 = 0.0245$. Now the primary double-zero bifurcation gives unacceptable $|\Delta\varepsilon_1| = 0.075$ differences, and the fold takes place at $\mathcal{O}(1)$ amplitudes. This indicates that nonlinear interactions of other modes

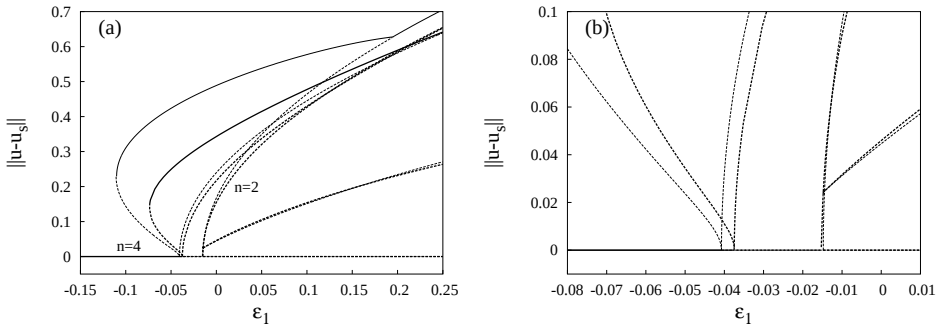

FIGURE 14. (a) Superposition of Fig. 11 and the bifurcation diagram obtained from the PDE system for $\varepsilon_2 = +0.0045$. (b) Detail of (a) for small amplitudes. The thick and thin lines correspond to the PDE and the ODE systems, respectively.

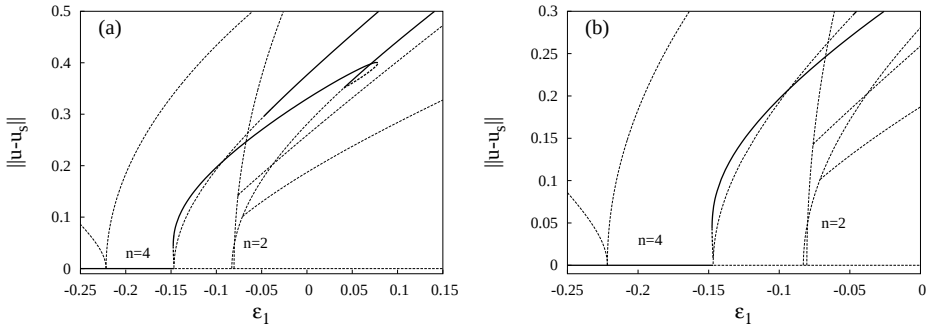

FIGURE 15. (a) Superposition of Fig. 3 and the bifurcation diagram obtained from the ODE system for $\varepsilon_2 = +0.0245$. (b) Detail of (a) for small amplitudes. The thick and thin lines correspond to the PDE and the ODE systems, respectively.

not considered in the model are already important. However, even in this case, the model maintains the main features at small amplitudes, namely, the character of the bifurcations on the $n = 4$ branch, and the first pitchfork bifurcation on the $n = 2$ branch of the PDEs. In fact, the amplitude equations do show all bifurcations in Fig. 3, including the instability point in the middle of one of the branches that bifurcate at $Ra = 9880$, which involves net drifting solutions, but these occurs for large values of the amplitudes, which are outside the validity of the amplitude equations.

7. **Conclusions.** We have introduced a numerical perturbation technique to determine the coefficients of the amplitude equations near bifurcations of spatio-temporal symmetric periodic solutions. This technique only requires an accurate time evolution code. In fact, the calculation of the adjoint problem can be avoided by imposing that the solutions of (24)-(30) be bounded. However, in this case the method is not so fast and requires minimizing the linear growth slope with respect to the parameters. In any event, the generalization of the Lindstedt-Poincaré technique results

to work very well for PDE systems. To our knowledge, no similar techniques have been developed in the literature for the precise calculation of the coefficients of the amplitude equations near bifurcation points in Floquet problems in PDEs. Symmetry arguments allow to guess the form of the amplitude equations, but not the numerical values of the coefficients, which can be essential to anticipate the range of validity of the approximation and to explain quantitative discrepancies. For instance, the poor comparison in Fig. 15 becomes clear noticing the large numerical value of the coefficient α_3. Empirical fitting can of course be always done, but this is not convincing enough and, in fact, can yield wrong results when the number of unknown coefficients is large. For example, since as mentioned above, the amplitude equations do contain all bifurcations shown in Figs. 2 and 3 (some of them for large values of the amplitudes, which are not acceptable), these two diagrams could be approximated reasonably well by appropriate (but wrong) selection of the coefficients.

In the case considered in this paper, the analysis of the amplitude equations confirms the numerical results. Any of the branches that bifurcate from the $\mathbb{D}_4$-symmetric basic solution, u_s, consist of time periodic orbits that exhibit no net drift. Namely, near the multiple (+1) bifurcation the dynamics is also restricted to the invariant manifolds $A_1 = \pm A_2$, and $A_3 = 0$, and therefore $\dot{\varphi} = 0$. Thus, due to the symmetry fourteen branches of periodic orbits without net azimuthal drift collapse at the triple $\mu = +1$ bifurcation point. However, it is necessary to consider the invariance of the system by rotations to determine the local coefficients of the amplitude equations.

Appendix A. **Solvability conditions.** The coefficients of the amplitude equations (20)-(22) are calculated imposing that the nonhomogeneous, linear problems (24), (26)-(30), possess T-periodic solutions (solvability condition), or equivalently (see below) that all solutions to these equations be bounded as $\tau \to \infty$ (elimination of secular terms). These equations can be written as

$$\mathcal{L}_0 \partial_\tau U = \mathcal{L} U + H - \sum_{j=1}^{5} b_j \mathcal{L}_0 U_j^0,$$

where

$$\mathcal{L} = \mathcal{L}_1 + \mathcal{B}(\cdot, u_s^0) + \mathcal{B}(u_s^0, \cdot), \tag{35}$$

$U_4^0 = \partial_\theta u_s^0$, $U_5^0 = \partial_\tau u_s^0$, and $H(\tau) = H(\tau + T)$.

Let the constant, invertible linear operator $\mathcal{L}_0$, and the T-periodic, linear operator $\mathcal{L}$ be such that the homogeneous equation

$$\mathcal{L}_0 \partial_\tau U = \mathcal{L} U, \quad U(0) = U_0 \tag{36}$$

defines a unique solution $U(\tau) = \mathcal{G}(\tau) U_0$, where, for each $\tau > 0$, the Green operator $\mathcal{G}(\tau)$ is a linear, compact, Fredholm operator in a Hilbert space $(E, \langle \cdot, \cdot \rangle)$. Note that the Floquet multipliers of (36) are the eigenvalues of $\mathcal{G}(T)$. Assume in addition that eq. (36) exhibits the Floquet multiplier $\mu = +1$ with (algebraic and geometric) multiplicity five, and that the remaining Floquet multipliers are within the unit circle, at a nonzero distance from the boundary.

Lemma 1. *The equation*

$$\mathcal{L}_0 \partial_\tau U = \mathcal{L} U + \tilde{H} \tag{37}$$

exhibits T-periodic solutions if and only if

$$\int_0^T \langle \tilde{H}, U_j^* \rangle \, d\tau = 0 \quad \textit{for } j = 1, \ldots, 5, \tag{38}$$

where U_j^* are five linearly independent, T-periodic eigenfunctions of the adjoint problem

$$-\mathcal{L}_0^\top \partial_\tau U^* = \mathcal{L}^\top U^*,$$

which also exhibits the Floquet multiplier $\mu = +1$ with multiplicity five; these eigenfunctions can be chosen such that $\int_0^T \langle U_j^*, \mathcal{L}_0 U_k \rangle \, d\tau = 1$ and 0 if $j = k$ and $j \neq k$, respectively. Here, $\top$ stands for the adjoint with respect to the inner product $\langle \cdot, \cdot \rangle$. Furthermore, if these conditions hold, then (37) possesses a five-dimensional, linear manifold of periodic solutions.

Proof. The statement that (37) exhibits T-periodic solutions if and only if (38) holds is proved by the argument in [6, p.206, theorem 7.3.2], after slight modifications. Adding the general T-periodic solution of (36) to a particular T-periodic solution of (37), the last statement follows. □

Lemma 2. *The solutions of the equation (37) are of the form*

$$U = \sum_{j=1}^{5} a_j \tau U_j^0 + V + E.S.T, \tag{39}$$

where $U_1^0, \ldots, U_5^0$ are five linearly independent periodic solutions of (36) associated with the Floquet multiplier $\mu = +1$, V is T-periodic, and $E.S.T$ denote exponentially small terms as $\tau \to \infty$. Thus, this system exhibits periodic solutions if and only if $a_j = 0$, $j = 1, \cdots, 5$.

Proof. Replace (39), ignoring E.S.T., into (37), to obtain that this latter equation holds provided that

$$\mathcal{L}_0 \partial_\tau V = \mathcal{L} V + H - \sum_{j=1}^{5} a_j \mathcal{L}_0 U_j^0.$$

□

Applying the preceding lemma, the constants a_j can be uniquely selected such that this problem possesses periodic solutions. Adding the general solution of the homogeneous version of (37), we readily obtain the E.S.T..

Note that $\int_0^T \langle \cdot, \cdot \rangle \, d\tau$ defines an inner product in the space of those time dependent functions defined in the domain of the operator $\mathcal{L}$ that are T-periodic. Also note that the problem giving U^* must be integrated backwards when dealing with the Navier-Stokes equations (or with any other parabolic problem).

Summarizing, imposing boundedness of the solutions of (37) is equivalent to impose that this equations possess T-periodic solutions. Each of these properties can be used to uniquely calculate the coefficients of the amplitude equations.

In order to apply all these to the linear problems in Sec. (5), the Hilbert space E is defined as the (L^2) space of those square integrable functions in $R_i < r < R_o$, $0 < \theta \leq 2\pi$, with the inner product

$$\langle u_1, u_2 \rangle = \frac{1}{2\pi} \int_0^{2\pi} \int_{R_i}^{R_o} (f_1 f_2 + \Theta_1 \Theta_2 + \psi_1 \psi_2) \, r dr d\theta, \tag{40}$$

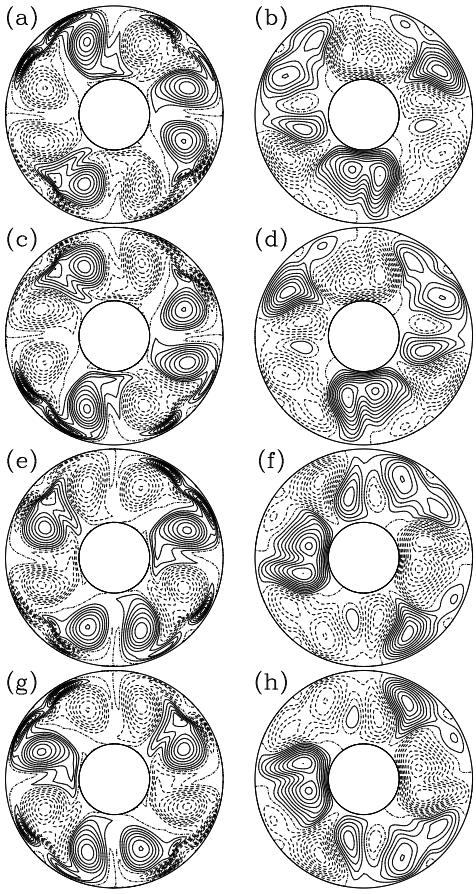

FIGURE 16. From left to right, (a), (b) instantaneous streamlines and temperature perturbation, respectively, for $U_1^*(0)$, (c), (d) for $U_1^*(T/2)$, (e), (f) for $U_2^*(0)$, and (g), (h) for $U_2^*(T/2)$. $Ra_c = 10385$, $\eta_c = 0.3255$.

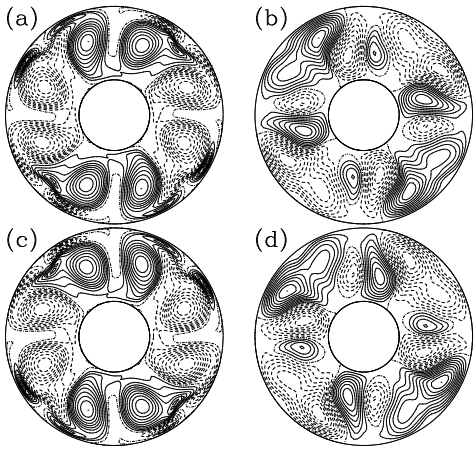

FIGURE 17. From left to right, (a), (b) instantaneous streamlines and temperature perturbation, respectively, for $U_3^*(0)$, and (c), (d) for $U_3^*(T/2)$. $Ra_c = 10385$, $\eta_c = 0.3255$.

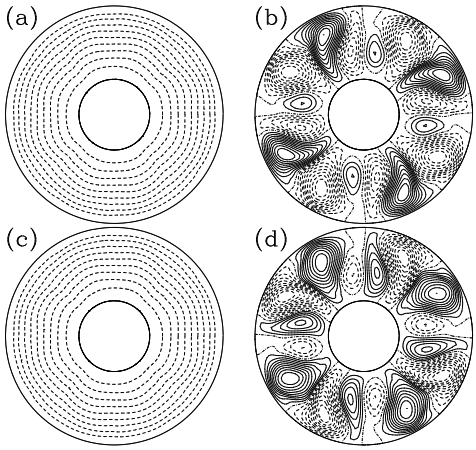

FIGURE 18. From left to right, (a), (b) instantaneous streamlines, and temperature perturbation, respectively, for $U_4^*(0)$, and (c), (d) for $U_4^*(T/2)$. $Ra_c = 10385$, $\eta_c = 0.3255$.

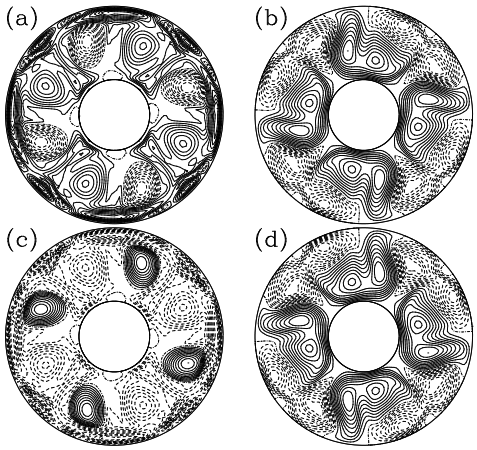

FIGURE 19. From left to right, (a), (b) instantaneous streamlines, and temperature perturbation, respectively, for $U_5^*(0)$, and (c), (d) for $U_5^*(T/2)$. $Ra_c = 10385$, $\eta_c = 0.3255$.

and the linear operator $\mathcal{L}$ is as defined in (35). Note that the range of the operator $\mathcal{G}$ is the subspace of those functions such that $\mathcal{L}u$ is square integrable and u satisfies the boundary conditions. The adjoint operator $\mathcal{L}^\top$ is obtained imposing that $\langle u_1, \mathcal{L}u_2\rangle = \langle \mathcal{L}^\top u_1, u_2\rangle$ for all u_1, u_2 in the range of $\mathcal{G}$. Using these, the definition (40), and that $P_\theta^\top = P_\theta$, $P_\theta f = f$, and $(1 - P_\theta)\psi = \psi$, we obtain upon repeated

integration by parts invoking the boundary conditions (6), $\mathcal{L}_0^\top = \mathcal{L}_0$ and

$$\mathcal{L}^\top u = \begin{pmatrix} \sigma\tilde{\Delta} & 0 & 0 \\ 0 & \Delta & -\sigma r^{-1} Ra\ \partial_\theta \\ 0 & (r^2 \ln\eta)^{-1}\partial_\theta & \sigma\Delta\Delta \end{pmatrix} \begin{pmatrix} f \\ \Theta \\ \psi \end{pmatrix} +$$

$$+ \begin{pmatrix} P_\theta\Big[\tilde{\Delta}\left(\psi\partial_\theta\psi_s/r\right) - \Theta\partial_\theta\Theta_s/r - \psi\partial_\theta\Delta\psi_s/r\Big] \\ -J(\psi_s,\Theta) + f_s\partial_\theta\Theta/r \\ (1-P_\theta)\Big[\Delta J(\psi,\psi_s) - J(\psi,\Delta\psi_s) - J(\Theta,\Theta_s)\Big] + \Delta\left(\left(f\partial_\theta\psi_s + f_s\partial_\theta\psi\right)/r\right) \\ -\left(f\partial_\theta\Delta\psi_s + \tilde{\Delta}f_s\partial_\theta\psi\right)/r \end{pmatrix},$$

where $u_s = (f_s, \Theta_s, \psi_s)$.

The T-periodic eigenfunctions U_j^* of the adjoint problem are shown in Figs. (16-19). They are ordered to be in correspondence to U_j^0. Each U_j^* has the same spatial and spatio-temporal symmetries as U_j^0. Because of these symmetries and those of $\tilde{H}$, each coefficient can be determined directly selecting the only U_j^* which does not verify identically the orthogonality condition (38).

Acknowledgments. The research by JS and MN has been supported by MEC-DGI (Grant FIS2004-01066), and Catalonia GENCAT (Grant 2005SGR01028), and that by JMV was partially supported by MEC-DGI (Grant MTM2004-03808), and NASA (Grant NNC04GA47G).

REFERENCES

[1] A. Alonso, M. Net, and E. Knobloch, *On the transition to columnar convection,* Phys. Fluids, **7** (1995), no. 5, 935–940.
[2] P. Chossat and G. Ioos, The Couette-Taylor problem. Springer, 1994.
[3] S. M. Cox, *Mode interactions in Rayleigh-Bénard convection*, Physica D, **95** (1996), 50–61.
[4] J. D. Crawford and E. Knobloch, *Symmetry and symmetry-breaking bifurcations in fluid mechanics*, Ann. Rev. Fluid Mech., **23** (1991), 341–387.
[5] Z. A. Daya, V. B. Deyirmenjian, S. W. Morris and J. R. de Bruyn, *Annular electroconvection with shear*, Phys. Rev. Lett., **80** (1998), 964–967.
[6] D. Henry, Geometric theory of semilinear parabolic equations. Springer, 1989.
[7] M. Ishiwatari, S-I. Takehiro, and Y-Y, Hayashi, *The effects of thermal conditions on the cell sizes of two-dimensional* convection, J. Fluid Mech., **281** (1994), 33–50.
[8] A. S. Landsberg, and E. Knobloch, *Direction-reversing traveling waves*, Phys. Lett. A, **159** (1991), 17–20.
[9] W. F. Langford, and D. D. Rusu, *Pattern formation in annular convection*, Physica A, **261** (1998), 188–203.
[10] J. S. W. Lamb, *k-symmetry and return maps of spacetime symmetric flows*, Nonlinearity, **11** (1998), 601–629.
[11] J. S. W. Lamb, I. Melbourne, and C. Wulff, B*ifurcation from periodic solutions with spatiotemporal symmetry, including resonances and mode interactions*, J. Differential Equations, **191** (2003), 377–407.
[12] M. Net, A. Alonso, and J. Sánchez, *From stationary to complex time-dependent flows in two-dimensional annular thermal convection at moderate Rayleigh numbers,* Phys. Fluids, **15** (2003), no. 5, 1314–1326.
[13] M. Net, and J. Sánchez, *Symmetric periodic orbits and global dynamics of quasi-periodic flows in an $O(2)$ equivariant system: Two-dimensional thermal convection.* Int.J. Bifurcation and Chaos., **15** (2005), no. 12, 3953–3972.
[14] D. Pino, I. Mercader, and M. Net. *Thermal and inertial modes of convection in a rapidly rotating annulus*, Phys. Rev. E, **61** (2000), no. 2, 1507–1517.

[15] J. Porter, and M. Silber, *Broken Symmetries and pattern formation in two-frequency forced Faraday waves.* Phys. Rev. Lett., **89** (2002), no. 8, 084501(4).

[16] A. M. Rucklidge, and M. Silber, *Bifurcations of periodic orbits with spatio-temporal symmetries*, Nonlinearity, **11** (1998), 1435–1455.

[17] A.M. Rucklidge, *Global bifurcations in the Takens-Bogdanov normal form with D_4 symmetry near the $O(2)$ limit*, Phys. Lett. A, **284** (2001), no. 2, 99–111.

[18] M. Silber, and A. C. Skeldon, P*arametrically excited surface waves: Two-frequency forcing, normal form symmetries, and pattern selection.* Phys. Rev. E, **59** (1999), no. 5, 5446–5455.

[19] J. Sánchez, M. Net, B. García-Archilla and C. Simó, *Newton-Krylov continuation of periodic orbits for Navier-Stokes flows*, J. Comput. Phys., **201** (2004), 13–33.

Received July 2005; revised June 2006.

E-mail address: sanchez@fa.upc.edu